Acta Crystallographica Section A
Foundations of Crystallography
ISSN 0108-7673

Received 29 November 2004
Accepted 29 March 2005

The prior-derived *F* constraints in the maximum-entropy method

Lukáš Palatinus‡ and Sander van Smaalen*

Laboratory of Crystallography, University of Bayreuth, Germany. Correspondence e-mail: smash@uni-bayreuth.de

The method of the prior-derived *F* constraints (PDC) enhances the quality of reconstructions of electron densities from X-ray diffraction data by the maximum-entropy method (MEM). The method concentrates on artifacts arising due to inaccurate extrapolation of non-measured data by the MEM. While these artifacts are unavoidable, when a flat prior is used, they can be effectively suppressed, if the prior information about the structure is known in the form of a procrystal prior electron density. The missing, usually high-angle, structure factors can be effectively substituted by the structure factors derived from the procrystal prior. This approach eliminates the occurrence of spurious peaks in the difference electron densities in the vicinity of the atomic positions. The method is illustrated with a simple one-dimensional example. Its use is then demonstrated on simulated data of oxalic acid dihydrate and on experimental data of sodium nitrite.

1. Introduction

The maximum-entropy method (MEM) is a general-purpose method for data analysis, pioneered mainly by the works of Jaynes, *e.g.* Jaynes (1957, 1979, 1986). The purpose of the method is to extract the maximum amount of information from the data, without introducing artifacts or assumptions based on models (Sivia, 1996). One of its applications in crystallography is the reconstruction of the electron density in the unit cell from X-ray diffraction data (Collins, 1982; Gilmore, 1996). By virtue of its properties, the MEM should be able to replace model-based refinements for the determination of advanced structural features, like disorder, anharmonic temperature displacements and the electron density in the chemical bond (multipole parameters), as well as the shapes of modulation functions of aperiodic crystals (Bagautdinov *et al.*, 1998; Dinnebier *et al.*, 1999; Wang *et al.*, 2001; van Smaalen *et al.*, 2003; Takata *et al.*, 1999). However, it has been pointed out that the reconstructed electron density [$\rho^{\rm MEM}(\mathbf{r})$] suffers from artifacts that are specific to the MEM (Jauch & Palmer, 1993; Jauch, 1994; de Vries *et al.*, 1996; Roversi *et al.*, 1998; Palatinus & van Smaalen, 2002). The magnitudes of the noise or spurious maxima in $\rho^{\rm MEM}(\mathbf{r})$ may be larger than the features of interest, especially so when the electron density in the chemical bond is studied. The most extensively analyzed example is silicon, for which the MEM may produce a local maximum in $\rho^{\rm MEM}(\mathbf{r})$ at the center of the Si—Si bond, which has been shown to be an artifact (Sakata & Sato, 1990; de Vries *et al.*, 1996). Several modifications of the MEM have been proposed that aim at repairing these problems.

Two main sources of errors can be identified, which produce artifacts in $\rho^{\rm MEM}(\mathbf{r})$. One type of error is related to series-termination effects, as is the result of the availability of only a finite (and often limited) number of reflections in any data set (Jauch, 1994). These artifacts can effectively be suppressed by reducing the dynamic range of the problem. The application of the maximum-entropy (MaxEnt) principle to the difference electron density (Papoular *et al.*, 1996) or to the valence electrons only (Roversi *et al.*, 1998) have been proposed as MaxEnt methods with a reduced dynamic range in reciprocal space. Alternatively, the use of a sufficiently informative reference electron density (prior) corresponds to a reduction of the dynamic range in direct space and also suppresses artifacts (de Vries *et al.*, 1996; Papoular *et al.*, 2002; Palatinus & van Smaalen, 2002).

The second type of error is due to the sensitivity of the MEM to the distribution of weights in the χ^2 constraint on the experimental data. Artifacts are produced in $\rho^{\rm MEM}(\mathbf{r})$ even if exact values for the standard uncertainties of the reflection intensities are available for the definition of the weights in the χ^2 constraint. The effect on χ^2 has been described in detail (Jauch, 1994; de Vries *et al.*, 1994; Iversen *et al.*, 1997). At convergence, those structure factors that are most sensitive to changes of the entropy are estimated incorrectly, in order to decrease the entropy as much as possible at lowest cost of constraint. These reflections are known as outliers. One or two outliers often account for a substantial part of χ^2, while the other reflections are over-fitted. This problem can be reduced by employing different weight schemes within the χ^2 constraint (de Vries *et al.*, 1994), or by using a constraint based on higher-order moments of the Gaussian error distribution than the second moment represented by the χ^2 constraint (de

‡ Present address: Institute of Physics, Academy of Sciences of the Czech Republic, 162 53 Prague, Czechia.

Vries *et al.*, 1994; Palatinus & van Smaalen, 2002). However, none of the MaxEnt methods reliably produces a density $\rho^{\rm MEM}(\mathbf{r})$ that is sufficiently accurate to enable the extraction of properties of the chemical bond from it, as is usually done for theoretical and multipole densities (Bader, 1990).

In the present contribution, we propose yet another modification to the constraints employed in the MEM, which we have called the prior-derived F constraints (PDC). A one-dimensional crystal is used to elucidate how the use of the PDC suppresses artifacts in $\rho^{\rm MEM}(\mathbf{r})$. The ability of MEM with PDC to extract the electron density in the chemical bond from good X-ray diffraction data is demonstrated for oxalic acid dihydrate (using simulated data) and sodium nitrate (using experimental data).

2. Method of prior-derived *F* constraints

In this work, the entropy S of the electron density in the unit cell $[\rho(\mathbf{r})]$ is defined as

$$S = -\sum_{k=1}^{N_{\rm pix}} \rho_k \ln(\rho_k/\tau_k), \qquad (1)$$

where $\rho_k = \rho(\mathbf{r}_k)$ are the electron-density values on a sufficiently fine grid over the unit cell ($k = 1, \ldots, N_{\rm pix}$). τ_k are the values of a reference electron density, the so-called prior. MaxEnt methods search for the distribution of density values $\{\rho_k\}$ that maximize S subject to the constraint of normalization of $\{\rho_k\}$ and subject to the constraint of fitting the diffraction data (Gilmore, 1996). The data can be incorporated using the F_2 constraint (Sakata & Sato, 1990),

$$C_{F_2} = -1 + \frac{1}{N_F}\sum_{\mathbf{H}} w_{\mathbf{H}} |F_{\rm obs}(\mathbf{H}) - F_{\rm MEM}(\mathbf{H})|^2, \qquad (2)$$

where $F_{\rm obs}(\mathbf{H})$ are the observed structure factors, including their phases, and $F_{\rm MEM}(\mathbf{H})$ is obtained by a discrete Fourier transform of $\{\rho_k\}$. $w_{\mathbf{H}}$ are the weights and the summation extends over all N_F reflections in the data set. The index 2 in C_{F_2} is used to emphasize that this constraint is just a special case of the general constraint of order n (Palatinus & van Smaalen, 2002). Using the method of undetermined Lagrange multipliers, the maximum of

$$Q = S - \lambda C_{F_2} \qquad (3)$$

is searched for variation of $\{\rho_k\}$ and λ. An analytical solution does not exist and iterative procedures have to be used to find $\rho^{\rm MEM}(\mathbf{r})$ (Sakata & Sato, 1990; Skilling & Bryan, 1984). Convergence is defined when C_{F_2} falls below its expectation value $\langle C_{F_2}\rangle = 0$ ($\langle\chi^2\rangle = 1$).

The simplest version of the MEM employs a flat prior ($\tau_k =$ average electron density) and weights based on the standard uncertainties ($\sigma_{\mathbf{H}}$) of the reflections ($w_{\mathbf{H}} = \sigma_{\mathbf{H}}^{-2}$). Artifacts in $\rho^{\rm MEM}(\mathbf{r})$ are large compared to the effects of chemical bonding on the electron density but they are small compared to $\rho(\mathbf{r})$ itself. Therefore, this method is only suitable to study properties with large variations of the electron density, like disorder and anharmonic temperature parameters.

Artifacts in $\rho^{\rm MEM}(\mathbf{r})$ will be smaller if the difference between the true (but unknown) electron density $\rho^{\rm true}(\mathbf{r})$ and the prior is smaller than the difference between $\rho^{true}(\mathbf{r})$ and the flat prior. If bonding electrons are the property of interest, the appropriate informative prior is the procrystal prior (de Vries *et al.*, 1996): $\tau(\mathbf{r}) = \rho^{\rm pro}(\mathbf{r})$. $\rho^{\rm pro}(\mathbf{r})$ is computed from the electron densities of free atoms, combined with temperature parameters and placed at positions obtained from the structure refinement within the independent-atom model (Papoular *et al.*, 2002). This choice of prior can be combined with different sets of weights in the constraint, *e.g.* with static weights as proposed by de Vries *et al.* (1994).

Even with optimal choices for the prior and the weights, $\rho^{\rm MEM}(\mathbf{r})$ is not sufficiently accurate to describe the effects of chemical bonding on the electron density. The origin of this problem can be identified as a feature of the MEM. The maximum of S [equation (1)] is obtained for $\rho_k = \tau_k$ for all pixels k. $\rho^{\rm MEM}(\mathbf{r})$ differs from $\tau(\mathbf{r})$ only as much as is necessary to reproduce the structure factors in the constraint [equation (2)]. The structure factors $[F_{\rm MEM}(\mathbf{H}')]$ of reflections $\mathbf{H}'$ for which experimental values are not available are extrapolated by the MEM. Because they are not constrained, erroneous estimates of the non-measured structure factors may be the result, leading to corresponding artifacts in $\rho^{\rm MEM}(\mathbf{r})$.

If no prior information on the electron density is available, the MEM estimates of the missing structure factors are the best possible estimates. For example, they are much better than the value zero, which is implicit to Fourier maps. However, if the re-distribution of valence electrons due to chemical bonding is the only unknown of the problem, then good estimates for the structure factors of high-angle reflections are provided by the procrystal prior, because valence electrons contribute to low-angle reflections only. $F_{\rm prior}(\mathbf{H}')$, as obtained by discrete Fourier transform of $\rho^{\rm prior}(\mathbf{r})$, thus provide good estimates for the true structure factors of high-angle reflections.

Based on these observations, we propose to append the constraint by extra terms for the non-measured reflections, with $F_{\rm prior}(\mathbf{H}')$ replacing $F_{\rm obs}(\mathbf{H})$ [equation (2)]:

$$C_{F_2}^{\rm PDC} = -1 + \frac{1}{N_{\rm all}}\sum_{\mathbf{H}} w_{\mathbf{H}} |F_{\rm obs}(\mathbf{H}) - F_{\rm MEM}(\mathbf{H})|^2 + \frac{1}{N_{\rm all}}\sum_{\mathbf{H}'} w_{\mathbf{H}'} |F_{\rm prior}(\mathbf{H}') - F_{\rm MEM}(\mathbf{H}')|^2, \qquad (4)$$

where $N_{\rm all} = N_F + N_{\rm prior}$ and $N_{\rm prior}$ is the number of reflections included in the sum over $\mathbf{H}'$. $C_{F_2}^{\rm PDC}$ then is used instead of C_{F_2} in equation (3). However, the convergence is not based on $C_{F_2}^{\rm PDC} < 0$, but instead the calculation is considered converged when the condition $C_{F_2} < 0$ [equation (2)] is fulfilled, thus ensuring a good fit of the resulting MEM density to the experimental data. Standard uncertainties are assigned to $F_{\rm prior}(\mathbf{H}')$ that are equal to the smallest standard uncertainty amongst the experimental data. Weights $w_{\mathbf{H}'}$ are based on these standard uncertainties, possibly combined with static

Table 1
Parameters of the Gaussians $G = A\exp[-(x-c)^2/2\sigma^2]$ used to construct the prior and true one-dimensional densities.

x, c and σ are expressed in pixels, whereas the scale of A is arbitrary. The width of the unit cell is 128 pixels, numbered from 0 at the origin to 127.

	Prior density			True density		
	A	σ	c	A	σ	c
A1	60	3.20	0	60	3.12	0
A2	50	3.20	64	50	3.12	64
A3	30	4.66	36	30	4.52	36
B1	0	–	–	0.5	11.31	15
B2	0	–	–	0.5	5.66	51

weighting. The sum over $\mathbf{H}'$ includes all reflections not available as experimental data up to some suitably chosen high-angle limit, *e.g.* $[\sin(\theta)/\lambda]_{\max} = 2.5$ Å^{-1}. We call the terms in the second sum in equation (4) the prior-derived F constraints (PDC).

The PDC ensure that the MEM estimates of the structure factors of high-angle reflections are close to $F_{\rm prior}(\mathbf{H}')$ and thus much closer to the true values than in the case of the MEM without the PDC. The PDC can only improve the MEM if accurate values for the structure factors ($F_{\rm obs}$) are available from experiment up to reasonably high scattering angles, *e.g.* $[\sin(\theta)/\lambda]_{\max} > 0.9$ Å^{-1}. This requirement on the experimental data is not different from the requirements imposed by good multipole refinements.

During the determination of the valence electron density by multipole refinements, a two-step procedure is sometimes employed. Initially, atomic positions and temperature factors are determined by refinement against high-angle reflections $[\sin(\theta)/\lambda > 0.9$ Å$^{-1}]$. With these parameters fixed, the multipole parameters are determined by a refinement against reflections with $\sin(\theta)/\lambda < 0.9$ Å^{-1} (Guillot *et al.*, 2001). Although entirely different methods, the MEM with PDC and this special procedure of multipole refinements work because of the same properties of electron densities and X-ray diffraction.

3. A one-dimensional model structure

A simple one-dimensional model is used to demonstrate the basic properties of the MEM with prior-derived F constraints. The electron density of a one-dimensional (1D) periodic structure was constructed by superimposing five Gaussian functions in the unit cell, resulting in the true density $\rho^{\rm true}$ (Table 1). Three Gaussians simulate the 1D analogons of atoms and two further Gaussians simulate the accumulation of density in bonds between the atoms (Fig. 1*a*). The procrystal prior $\rho^{\rm pro}$ was constructed from the three Gaussians representing atoms with renormalized widths in order to obtain the same number of electrons in $\rho^{\rm true}$ and $\rho^{\rm pro}$ (Table 1 and Fig. 1*b*). An inversion center was placed at the origin of the unit cell. The densities were sampled on a grid with 128 points.

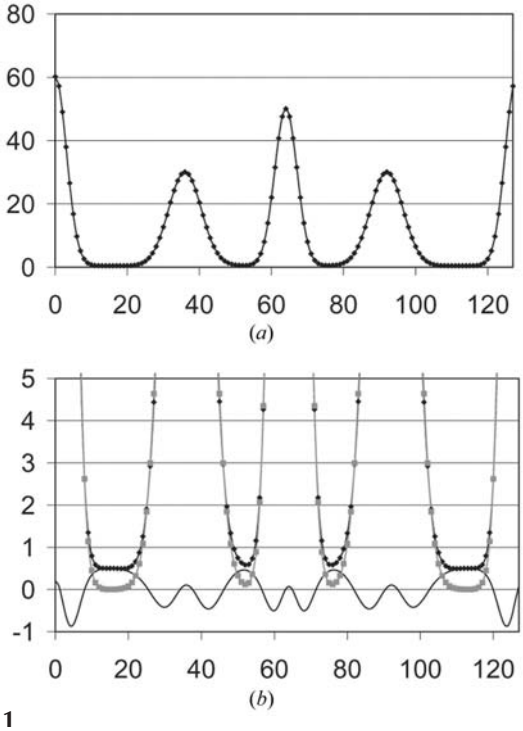

Figure 1
(*a*) One unit cell of the true one-dimensional density sampled on the grid with 128 pixels. (*b*) The exaggerated low-density region of the densities. Black diamonds: $\rho^{\rm true}$; grey squares: $\rho^{\rm pro}$; bold line: $\rho^{\rm true} - \rho^{\rm pro}$.

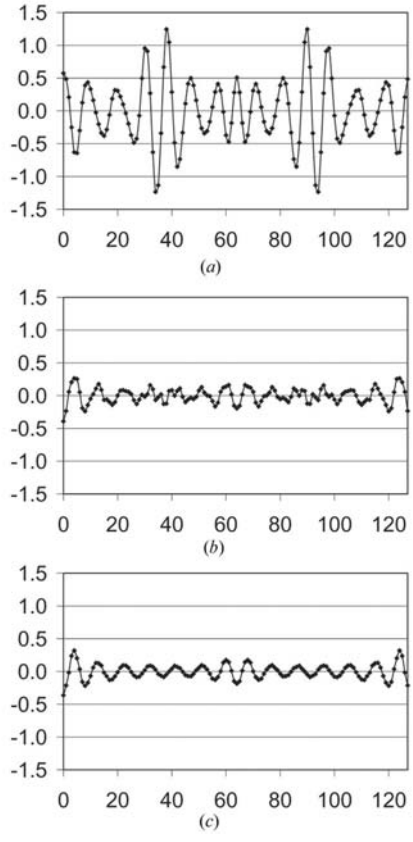

Figure 2
The difference densities $\rho^{\rm diff} = \rho^{\rm MEM} - \rho^{\rm true}$ from the calculations (*a*) f12p0, (*b*) f12p32, (*c*) f12p48. The lines connecting the points serve as a guide for eye.

ρ^{pro} is close to ρ^{true}. It is the task of the MEM to reconstruct the small differences of the order of 1% of the total density. This is analogous to the real cases of 3D crystals, where the procrystal prior density is available and only the deformations due to chemical bonding remain to be inferred.

Nine different MaxEnt optimizations were performed with the computer program *BayMEM* (van Smaalen *et al.*, 2003) using the Cambridge algorithm (Skilling & Bryan, 1984) and with ρ^{pro} as the prior density. Three sets of simulated data were created, by selecting all structure factors $F_{true}(h)$ with index h up to 12, 20 and 28, respectively, as they were obtained by discrete Fourier transform of ρ^{true}. Standard uncertainties $\sigma = 0.01$ were assigned to all structure factors. MEM calculations were performed with each data set for the case without PDC as well as with PDC up to $F_{prior}(32)$ and $F_{prior}(48)$, respectively. The calculations are denoted with the letter 'f' followed by the number of structure factors in the input data set and the letter 'p' followed by the highest index of the added PDC. For example, f20p48 denotes a calculation with structure factors up to $F_{true}(20)$ in the data and the remaining structure factors up to $F_{prior}(48)$ added as PDC.

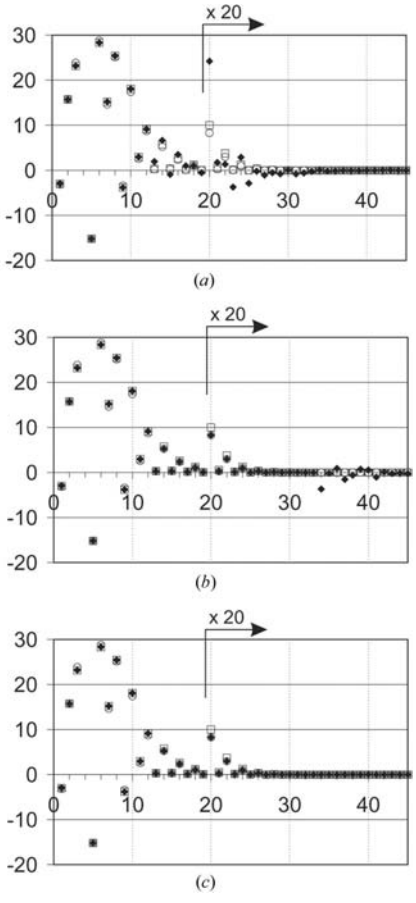

Figure 3
The structure factors F_{MEM} (filled diamonds) corresponding to ρ^{MEM} from calculations (*a*) f12p0, (*b*) f12p32, (*c*) f12p48. F_{true} (open squares) and F_{pro} (open circles) are shown in each plot for comparison. Values of structure factors with indices higher than 19 are multiplied by 20. Structure factor $F(4)$ has a value of approximately 64 and is not shown in the plots.

Table 2
Entropy of ρ_{MEM} from different calculations.

	PDC up to:		
Observed data up to:	0	$F(32)$	$F(48)$
$F(12)$	−1.53815	−1.88067	−1.88290
$F(20)$	−1.74731	−1.78002	−1.78153
$F(28)$	−1.76185	−1.76343	−1.76498

The resulting difference densities $\rho^{diff} = \rho^{MEM} - \rho^{true}$ are shown in Figs. 2, 4 and 6. The corresponding MEM structure factors $F_{MEM}(h)$ are compared to $F_{true}(h)$ in Figs. 3, 5 and 7. ρ^{diff} obtained without the prior-derived F constraints shows large wavy structures that are comparable in amplitude to the difference between the prior and true densities. The difference densities are dominated by a few frequencies. These frequencies correspond to the missing structure factors that have been most badly estimated. The difference between the values $F_{true}(h)$ and $F_{MEM}(h)$ of these structure factors is responsible for the occurrence of waves in the difference density with periodicity $1/h$ in the unit cell and with amplitude proportional to $|F_{true}(h)| - |F_{MEM}(h)|$. As an example, the most prominent structure in ρ^{diff} of the calculation f20p0 (Fig. 4*a*) is the wave with frequency 21, which corresponds to the overestimated value of $F(21)$ (Fig. 5*a*). The incorrect estimates

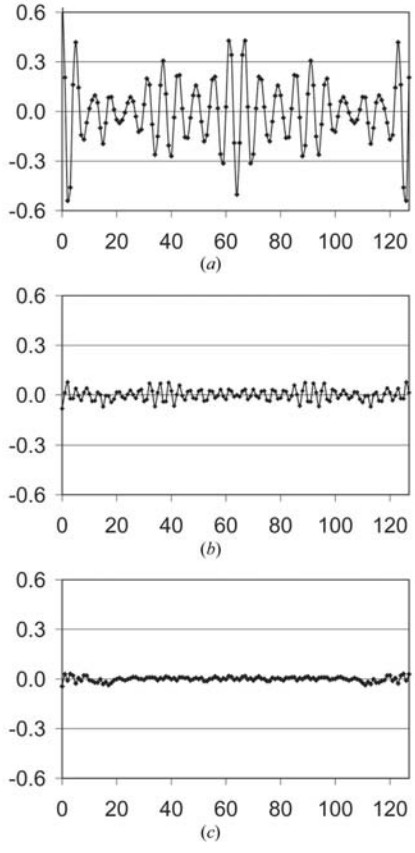

Figure 4
The difference densities $\rho^{diff} = \rho^{MEM} - \rho^{true}$ from the calculations (*a*) f20p0, (*b*) f20p32, (*c*) f20p48. The lines connecting the points serve as a guide for eye.

Table 3
Results of the calculations based on the simulated data sets n0r100, n1r100 and n2r100 of oxalic acid.

Calculation	C value	$\rho_{\rm diff}^{\rm min}$ (e Å^{-3})	$\rho_{\rm diff}^{\rm max}$ (e Å^{-3})
n0r100 without PDC	0.0057	−0.376	0.284
n0r100 with PDC	0.0034	−0.017	0.023
n1r100 without PDC	0.0157	−0.371	0.447
n1r100 with PDC	0.0138	−0.060	0.061
n2r100 without PDC	0.0358	−0.540	0.599
n2r100 with PDC	0.0344	−0.201	0.164

of the values of $F(21)$ and other structure factors are produced by the MEM because they increase the entropy of $\rho^{\rm MEM}$ compared to the entropy of the map with correct values of the structure factors. This can be seen by comparing the entropy of $\rho^{\rm MEM}$ with unconstrained high-order structure factors and the entropy of $\rho^{\rm MEM}$ with high-order structure factors constrained *via* PDC (Table 2). The entropy of the former is always higher than the entropy of the latter.

Calculations with the PDC and with 20 and 28 observed structure factors produce results with much lower values of $\rho^{\rm diff}$ as compared to the calculations without the PDC because the high-order structure factors are constrained to $F_{\rm prior}(h)$, which are very close to $F_{\rm true}(h)$ (Figs. 3, 5, 7). Calculations with the PDC up to $F(32)$ still show a high-frequency noise, which can be correlated with the overestimated values of the unconstrained structure factors above $F(32)$ (Figs. 5*b*, 7*b*). If PDC up to $F(48)$ are added, the resulting $\rho^{\rm MEM}$ shows only very small deviations from $\rho^{\rm true}$ (Figs. 4*c* and 6*c*). The remaining discrepancies are due to the fact that the MEM does not fit the low-order structure factors exactly. Nevertheless, the remaining errors in $\rho^{\rm diff}$ from the calculations f20p48 and f28p48 are smaller than 0.05 in absolute value, while the deformation density $\rho^{\rm true} - \rho^{\rm pro}$ has minimum −0.86 and maximum 0.50. Thus the MEM with PDC is able to reconstruct the difference between the $\rho^{\rm true}$ and $\rho^{\rm pro}$ with an average accuracy of a few percent.

The calculations f12p32 and f12p48 demonstrate the limitations of the method of the prior-derived F constraints. If all structure factors $F(h)$ for $h > 12$ are replaced by $F_{\rm prior}(h)$, then errors with a dominant frequency of 14 are found in the resulting difference densities (Figs. 2*b*, 2*c*). This is the result of the fact that $F_{\rm prior}(14) = 5.25$ is significantly different from $F_{\rm true}(14) = 5.76$. The value of $F_{\rm MEM}(14)$ is constrained to the value of $F_{\rm prior}(14)$ and the difference between $F_{\rm prior}$ and $F_{\rm true}$ is responsible for the artifacts in $\rho^{\rm diff}$. This error is induced by the incompleteness of the data and cannot be avoided by the data processing. Such a limited data set is not suitable for accurate reconstructions of the electron density.

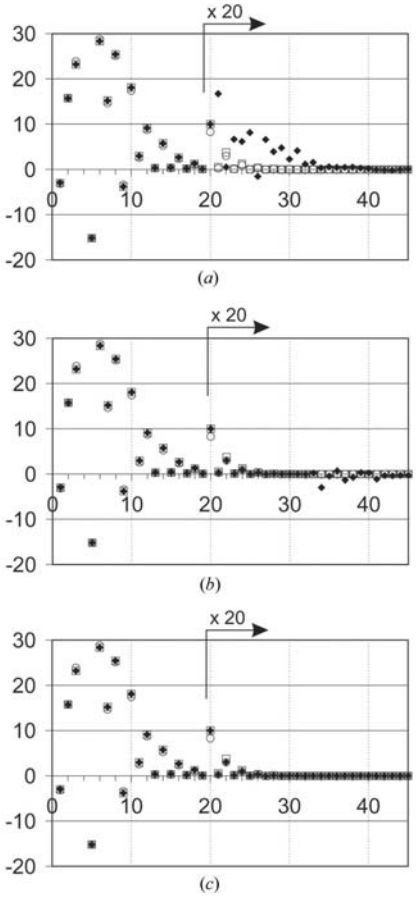

Figure 5
The structure factors $F_{\rm MEM}$ (filled diamonds) corresponding to $\rho_{\rm MEM}$ from calculations (*a*) f20p0, (*b*) f20p32, (*c*) f20p48. Other description as in Fig. 3.

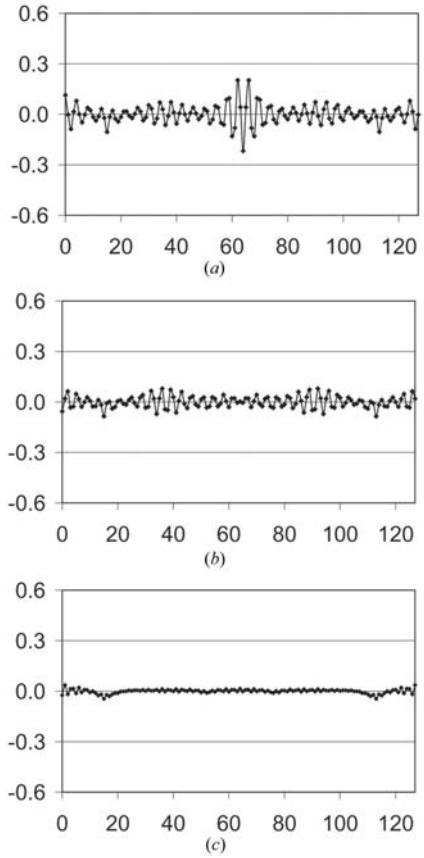

Figure 6
The difference densities $\rho^{\rm diff} = \rho^{\rm MEM} - \rho^{\rm true}$ from the calculations (*a*) f28p0, (*b*) f28p32, (*c*) f28p48. The lines connecting the points serve as a guide for the eye.

4. Simulated data for oxalic acid

The MEM with PDC was applied to simulated data for oxalic acid dihydrate in order to investigate the effects of the PDC on realistic data under controlled conditions.

A procrystal density ($\rho^{\rm pro}$) was constructed from spherical atoms combined with temperature parameters and placed at positions obtained from a standard refinement. The true electron density ($\rho^{\rm true}$) was then defined as the sum of $\rho^{\rm pro}$ and the static deformation density $\rho^{\rm def}$ as obtained from the multipole model by Šlouf (2001). All densities were sampled on a grid of $64 \times 32 \times 128$ pixels. Details of this model together with the method to generate simulated data from $F_{\rm calc}$ modified by Gaussian noise of various magnitudes are described in Palatinus & van Smaalen (2002) (hereafter denoted Paper I).

It was shown in Paper I that the use of the procrystal prior density enhances the performance of the MEM strongly compared to the MEM with a uniform prior, but that the resulting maps are not artifact-free either. To demonstrate the functionality of the PDC, the method was applied to the data sets n0r100, n1r100 and n2r100 [n0, n1 and n2 denoting increasing levels of noise, and r100 denoting a resolution of $(\sin\theta/\lambda)_{\rm max} = 1.00$ Å^{-1}; for details see Paper I]. Two calculations were performed on each data set. The first calculation was performed using the classical MEM formalism with the procrystal prior, the Cambridge algorithm (Skilling & Bryan, 1984) and static weighting with weights $w = |\mathbf{H}|^{-4}$ for data set n2r100 and $w = |\mathbf{H}|^{-5}$ for data set n1r100 [de Vries *et al.* (1994) and equation (13) in Paper I]. These weights produced the best results according to the *C*-value criterion applied to $\rho^{\rm MEM}$ [equation (12) and Table 5 in Paper I]. The second calculation was performed with the same algorithm and static weighting, but with PDC up to $\sin\theta/\lambda = 2.5$ Å^{-1} added to the experimental data. A uniform standard uncertainty of $\sigma_{\rm PDC} = 0.02$ was assigned to all reflections in the PDC.

The results of the calculations are summarized in Table 3. Sections through the difference electron density $\rho^{\rm diff} = \rho^{\rm MEM} - \rho^{\rm true}$ are shown in Figs. 8, 9 and 10 for the data sets n0r100, n1r100 and n2r100, respectively. Note that the data set n0r100 is noiseless, and the data sets n1r100 and n2r100 were constructed to approximately correspond to very accurate (n1r100) and moderately accurate (n2r100) experimental data sets. The results clearly show that the use of PDC

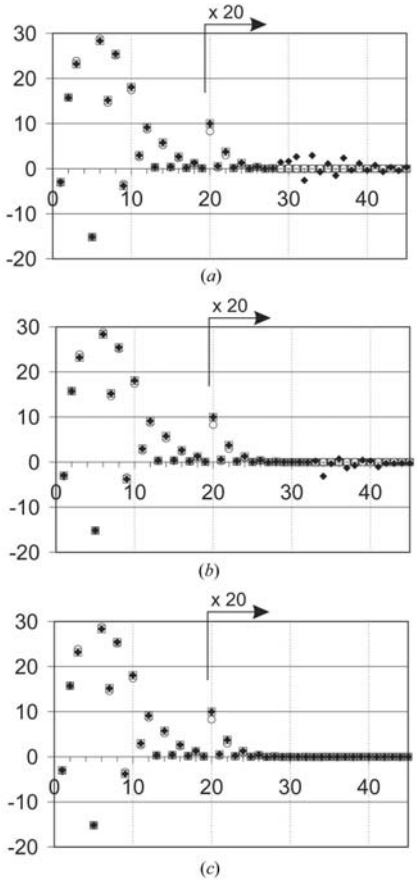

Figure 7
The structure factors $F_{\rm MEM}$ (filled diamonds) corresponding to $\rho_{\rm MEM}$ from calculations (*a*) f28p0, (*b*) f28p32, (*c*) f28p48. Other description as in Fig. 3.

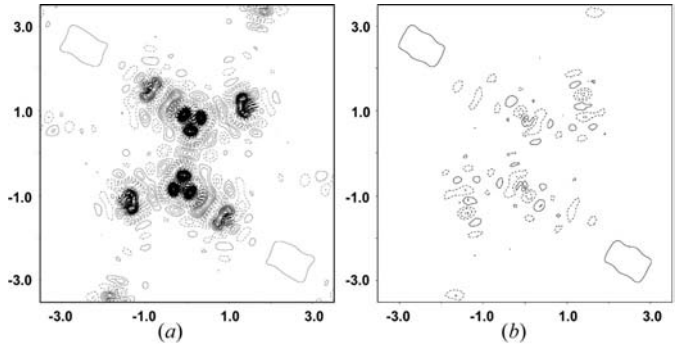

Figure 8
Sections of the difference density $\rho^{\rm diff} = \rho^{\rm MEM} - \rho^{\rm true}$ of oxalic acid dihydrate in the plane of the oxalic acid molecule, data set n0r100. (*a*) Calculation without the PDC. $\rho_{\rm min} = -0.342$ e Å^{-3}, $\rho_{\rm max} = 0.256$ e Å^{-3}. (*b*) Calculation with the PDC up to $\sin(\theta)/\lambda = 2.5$ Å^{-1}. $\rho_{\rm min} = -0.016$ e Å^{-3}, $\rho_{\rm max} = 0.014$ e Å^{-3}. Cambridge algorithm, no static weighting. Contours in both maps are drawn at intervals of 0.005 e Å^{-3}.

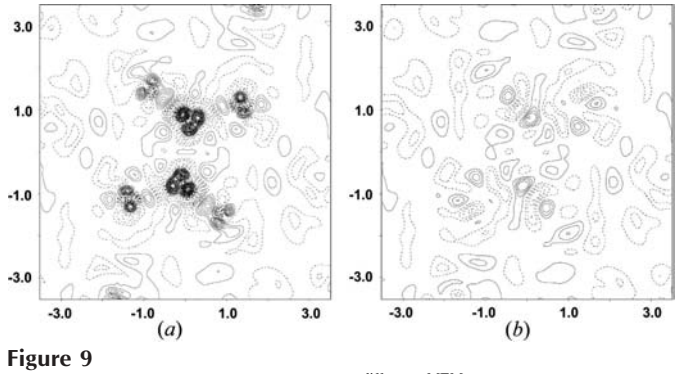

Figure 9
Sections of the difference density $\rho^{\rm diff} = \rho^{\rm MEM} - \rho^{\rm true}$ of oxalic acid dihydrate in the plane of the oxalic acid molecule, data set n1r100. (*a*) Calculation without the PDC. $\rho_{\rm min} = -0.144$ e Å^{-3}, $\rho_{\rm max} = 0.392$ e Å^{-3}. (*b*) Calculation with the PDC up to $\sin(\theta)/\lambda = 2.5$ Å^{-1}. $\rho_{\rm min} = -0.048$ e Å^{-3}, $\rho_{\rm max} = 0.051$ e Å^{-3}. Cambridge algorithm, static weighting, $w(\mathbf{H}) = |\mathbf{H}|^{-5}$. Contours in both maps are drawn at intervals of 0.01 e Å^{-3}.

improves the quality of the MEM reconstructions significantly. The difference density from the calculation without the PDC contains sharp peaks around the atomic positions. In the calculation with the PDC, these sharp artifacts disappear, the overall amount of noise decreases and the noise is distributed more uniformly. The deformation density $\rho^{\rm def} = \rho^{\rm MEM} - \rho^{\rm pro}$ obtained from the calculations is in perfect agreement with the true deformation density and is suitable for a quantitative analysis of the bonding interactions (Fig. 11).

5. Sodium nitrite

Sodium nitrite has a ferroelectric structure down to low temperatures. Recently, high-quality X-ray data were measured at $T = 30$ K up to a resolution of $(\sin\theta/\lambda)_{\rm max} = 1.125$ Å^{-1}, and they were analyzed by multipole refinements (Gohda *et al.*, 2000). Here we report the results of the MEM with PDC applied to these data. A procrystal prior for $NaNO_2$ was constructed from independent atoms with positions and displacement parameters obtained from a standard refinement on independent spherical atoms, employing the method of Papoular *et al.* (2002). MEM calculations were performed using the Cambridge algorithm (Skilling & Bryan, 1984), and several weighting schemes (de Vries *et al.*, 1994) were tested. Static weights $w(\mathbf{H}) = |\mathbf{H}|^{-3}$ were chosen for the final calculations reported here, because they produced a distribution of normalized residuals closest to the expected Gaussian distribution (Palatinus & van Smaalen, 2002).

Calculations were made without PDC and with PDC up to $\sin\theta/\lambda = 2.5$ Å^{-1}, resulting in MEM densities denoted as $\rho^{\rm noPDC}$ and $\rho^{\rm PDC}$, respectively. The difference density $\rho^{\rm noPDC}_{\rm def} = \rho^{\rm noPDC} - \rho^{\rm pro}$ contains sharp peaks around the atomic positions, while $\rho^{\rm PDC}_{\rm def} = \rho^{\rm PDC} - \rho^{\rm pro}$ is smooth (Fig. 12), thus showing the improvements of the MEM electron density on the introduction of PDC.

A comparison of $\rho^{\rm PDC}_{\rm def}$ with the static deformation density ($\rho^{\rm mult}_{\rm def}$) from the multipole model (Fig. 12*c*) shows a close qualitative resemblance between the two maps. Both maps exhibit the important expected features around the NO_2 group. However, differences are also found, for example the occurrence of the positive difference density around the Na site and the smaller height of the maxima around the NO_2 anion. At present, we have no detailed understanding of the origin of the discrepancies between $\rho^{\rm PDC}_{\rm def}$ and $\rho^{\rm mult}_{\rm def}$, but several possible reasons can be proposed.

(i) Six strong reflections were heavily affected by extinction and were excluded from the data set. The missing reflections may affect the MEM and multipole refinements in different ways.

(ii) The MEM, by virtue of its properties, tends to underestimate the deviation from the prior. However, this underestimation is always within the limits given by the data.

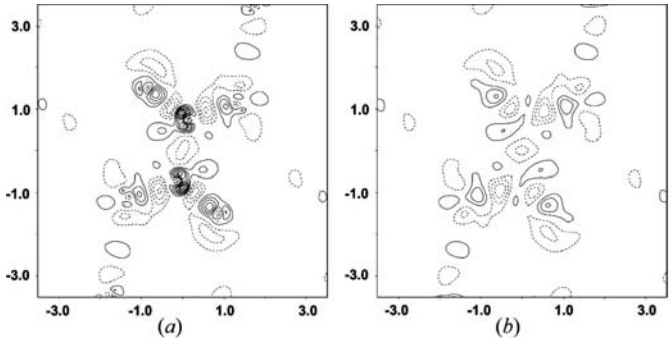

Figure 10
Sections of the difference density $\rho^{\rm diff} = \rho^{\rm MEM} - \rho^{\rm true}$ of oxalic acid dihydrate in the plane of the oxalic acid molecule, data set n2r100. (*a*) Calculation without the PDC. $\rho_{\rm min} = -0.210$ e Å^{-3}, $\rho_{\rm max} = 0.505$ e Å^{-3}. (*b*) Calculation with the PDC up to $\sin(\theta)/\lambda = 2.5$ Å^{-1}. $\rho_{\rm min} = -0.193$ e Å^{-3}, $\rho_{\rm max} = 0.161$ e Å^{-3}. Cambridge algorithm, static weighting, $w(\mathbf{H}) = |\mathbf{H}|^{-4}$. Contours in both maps are drawn at intervals of 0.05 e Å^{-3}.

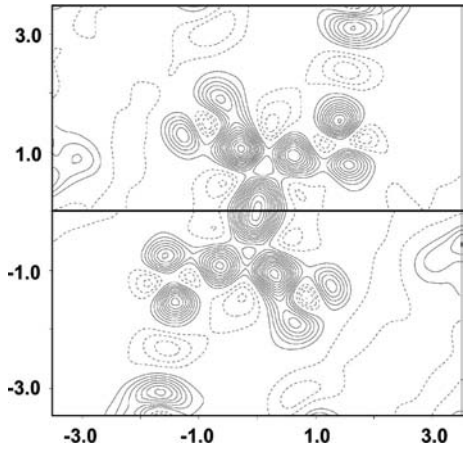

Figure 11
Comparison of the deformation densities $\rho^{\rm def}_{\rm MEM} = \rho^{\rm MEM} - \rho^{\rm pro}$ (lower half) and $\rho^{\rm def}_{\rm true} = \rho^{\rm true} - \rho^{\rm pro}$ (upper half) of oxalic acid dihydrate in the plane of the oxalic acid molecule. The center of the molecule lies in the middle of the figure and contains an inversion center. $\rho^{\rm def}_{\rm MEM}$ calculated with the data set n1r100, Cambridge algorithm, static weighting, $w(\mathbf{H}) = |\mathbf{H}|^{-5}$, and PDC up to $\sin(\theta)/\lambda = 2.5$ Å^{-1}. Contours are drawn at intervals of 0.04 e Å^{-3}.

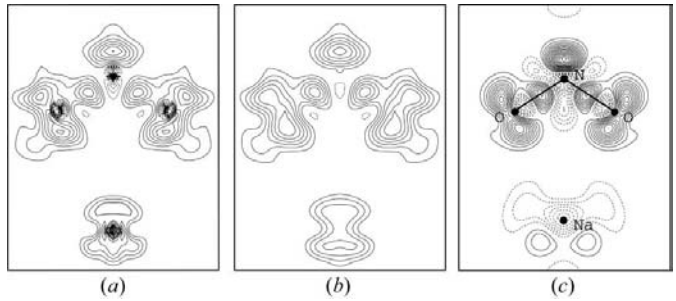

Figure 12
Sections of the deformation densities of sodium nitrite in the plane of the NO_2 group and Na atom. (*a*) $\rho^{\rm MEM} - \rho^{\rm pro}$, calculation without the PDC. $\rho_{\rm min} = -0.931$ e Å^{-3}, $\rho_{\rm max} = 0.488$ e Å^{-3}. (*b*) $\rho^{\rm MEM} - \rho^{\rm pro}$, calculation with the PDC up to $\sin(\theta)/\lambda = 2.5$ Å^{-1}. $\rho_{\rm min} = -0.083$ e Å^{-3}, $\rho_{\rm max} = 0.347$ e Å^{-3}. (*c*) Multipole deformation density [reprinted from Gohda *et al.* (2000)]. Contours in all plots at intervals of 0.05 e Å^{-3}, zero contour omitted.

(iii) The structure of $NaNO_2$ is non-centrosymmetric. The difference between $\rho_{\rm def}^{\rm PDC}$ and $\rho_{\rm def}^{\rm mult}$ can be caused by the inaccuracies of the phases of the structure factors determined from the refinement with spherical atoms. This source of inaccuracies will always be present if non-centrosymmetric structures are described by a model with spherical atoms (Souhassou *et al.*, 1991).

These problems, especially the latter one, could be at least partially eliminated by the use of a prior based on the multipole electron density instead of the procrystal prior (Roversi *et al.*, 1998, 2002). However, it is emphasized that the purpose of the present work is to establish the PDC as an extension of the MEM rather than to solve all discrepancies between the MEM and multipole refinements. The analysis of the origin of the discrepancies will be the subject of separate research.

6. Discussion

The method of prior-derived F constraints is based on the observation that the main errors in the MEM reconstructions of the electron densities with the procrystal prior originate from incorrect estimates of the MEM-extrapolated values of those structure factors that are not included in the data set. The errors can be reduced by replacing these missing structure factors by those derived from the prior electron density. This method can be successful only if the additional structure factors are very close to the true structure factors. For this reason, the MEM with PDC should be applied only to the high-resolution data sets, *e.g.* for data measured up to $\sin(\theta)/\lambda = 0.9$ Å^{-1} or more. The intensities of the high-angle reflections depend mostly on the electron density close to the atomic cores. This density is not influenced by the chemical bonding and is therefore almost the same in both the real and the procrystal electron densities. Thus, the differences between the real structure factors and the structure factors derived from the prior decrease with increasing $\sin(\theta)/\lambda$.

On the basis of the remarks made in the previous paragraph, one can roughly estimate the upper limit of the errors induced in the MEM reconstruction by the introduction of the PDC. The errors are caused by approximating the true structure factors by structure factors derived from the prior. It is reasonable to suppose that the largest difference $|F_{\rm true} - F_{\rm PDC}|$ will be smaller than the largest difference $|F_{\rm true} - F_{\rm prior}|$ close to the limit of the angular resolution; the latter can be estimated from the experiment as the value of $|F_{\rm obs} - F_{\rm prior}|$. The error induced by the PDC in the MEM reconstruction will be roughly equal to this difference.

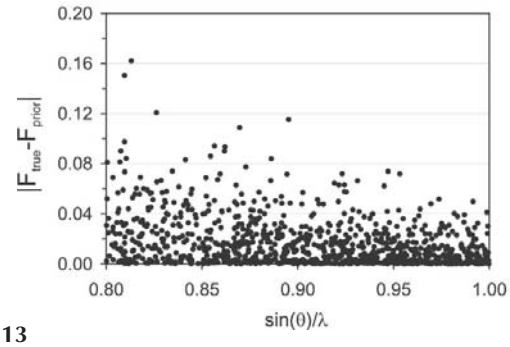

Figure 13
Distribution of $|F_{\rm true} - F_{\rm prior}|$ for the simulated data of oxalic acid dihydrate (data set n0r100) in the range $\sin\theta/\lambda \in \langle 0.8, 1.0$ Å$^{-1}\rangle$.

Table 4
Maximal differences between MEM densities $\rho_{\rm MEM}^{\rm PDC}$ of sodium nitrite depending on $\sigma^{\rm PDC}$.

The reference density is $\rho_{\rm MEM}^{\rm PDC}$ obtained with $\sigma^{\rm PDC} = 0.0005$.

$\sigma_{\rm PDC}$	$\rho_{\rm diff}^{\rm min}$ (e Å^{-3})	$\rho_{\rm diff}^{\rm max}$ (e Å^{-3})
0.001	−0.011	0.029
0.005	−0.072	0.0115
0.010	−0.079	0.085
0.020	−0.076	0.133
0.050	−0.083	0.084
0.100	−0.093	0.082
0.200	−0.099	0.075
0.500	−0.143	0.219
1.000	−0.288	0.404

An application of this method to estimate the errors is difficult in the case of the 1D example because the number of structure factors is limited. However, even here the method yields a reasonable estimate. The average value of $|F_{\rm obs} - F_{\rm prior}|$ for the three $F_{\rm obs}$ with highest index is 0.49, 0.09 and 0.002 for the data sets f12, f20 and f28, respectively. These numbers are also the estimates of the amplitude of the errors in the MEM reconstruction. The true maximum amplitude $(\rho_{\rm max}^{\rm diff} - \rho_{\rm min}^{\rm diff})/2$ is 0.32, 0.04 and 0.04 for the three data sets, respectively. In the first two cases, the estimated errors are quite good approximations to the true errors. In the case of the data set with the highest resolution (f28), the true error is much larger than the estimate. This is caused by the fact that, in this case, the other sources of error contribute to the total error much more than the PDC.

A similar analysis was performed on the simulated data of oxalic acid dihydrate. The differences $|F_{\rm obs} - F_{\rm prior}|$ for the data set n0r100 are plotted in Fig. 13 in the interval $\sin\theta/\lambda \in \langle 0.9, 1.0$ Å$^{-1}\rangle$. If the upper envelope of the absolute differences is extrapolated to higher angles, the expected error can be estimated to be close to 0.04 e Å^{-3}. The true error amplitude in the data set n0r100 is 0.02 e Å^{-3} (Table 3), which lies well within the estimated limit. The errors in the other two data sets are much larger due to the noise present in the data sets (Table 3). This observation confirms the underlying assumption of the PDC, according to which the error introduced by the use of the PDC is much smaller than the errors caused by the other sources, mainly by the noise in the data.

If the same error analysis is performed on the experimental data of sodium nitrite and if the experimental errors present in the data are taken into account, the error due to the introduction of the PDC in the MEM calculation can be estimated to be below 0.07 e Å^{-3}.

The constraint $C_{F_2}^{\rm PDC}$ [equation (4)] has two components, one based on the experimental data and one based on the model. The relative weighting of the two components is not defined by the theory. In practice, however, the exact definition of the weights is not critical. Since $F^{\rm PDC}$ are assumed to be

very accurate, the weights can theoretically be arbitrarily large, the true value being limited just by the limitations in handling small and large numbers by the computer. The large weights do not cause any problems in the convergence because the PDC term in $C_{F_2}^{\rm PDC}$ [the rightmost term in equation (4)] is exactly fulfilled at the beginning of the iteration. Table 4 shows the differences between MEM calculations of the density of sodium nitrite using different weighting of the PDC. The MEM reconstructions using various weights of the PDC differ only very little (with a maximum difference of about 0.1 e Å^{-3}) for a broad interval of $\sigma^{\rm PDC}$ between 0.0005 and 0.2. If $\sigma^{\rm PDC}$ becomes larger than 0.2, it allows sizeable artifacts to develop in the density, as illustrated in Table 4 by the increased differences for $\sigma^{\rm PDC} = 0.5$ and $\sigma^{\rm PDC} = 1.0$. The differences between the reconstructions with various $\sigma^{\rm PDC}$ are always confined to the vicinity of the atomic positions. We assigned uniform weights to all $F^{\rm PDC}$ approximately equal to the largest weight in the experimental data. In the case of sodium nitrite, this corresponds to $\sigma^{\rm PDC} = 0.01$. This assignment proved to be a good choice both for the accuracy of the result and for the optimization of the computation time.

It has been argued that the only proper prior electron density is the one based on a non-spherical multipolar model (Roversi *et al.*, 2002). The MEM calculations on the simulated data of oxalic acid dihydrate presented here show that very good reconstructions can be obtained also from a spherical model. On the other hand, the reconstructed densities of $NaNO_2$ show substantial differences between the MEM electron density and the multipolar model that might be amended by a multipolar prior. The question about the necessary form of the prior therefore still remains open. However, it should be emphasized that the problem that is addressed by the PDC is independent of the precise nature of the prior density. The difference between the multipolar and procrystal densities is contained almost exclusively in the low-angle structure factors, while the MEM with PDC addresses the high-angle structure factors and the effect addressed by the MEM with PDC will be present in calculations with both the procrystal and multipolar prior densities.

The 'valence-only MEM' (Roversi *et al.*, 1998) is another method aiming to suppress the artifacts that arise due to the missing high-angle structure factors in the constraints. In this method, the core electrons are kept fixed and are not subject to the entropy maximization. The remaining valence density has a lower dynamic range and its high-angle structure factors are virtually zero. Keeping the core electrons fixed is a much stronger restriction than fixing only the high-angle structure factors. If applicable, this method can certainly produce accurate density reconstructions. However, the valence-only MEM also relies on the exact knowledge of the displacement parameters. Therefore, if the displacement parameters cannot be determined with sufficient accuracy (for example due to the anharmonicity of the displacements or complex disorder), the applicability of the valence-only MEM is limited. The MEM with PDC also makes use of the displacement parameters, but in a less restrictive manner. This makes the MEM with PDC applicable to a wider variety of problems. An extensive study would be required to establish the differences in performance and applicability of the two methods.

7. Conclusions

The prior-derived *F* constraints have been introduced into the MEM for reconstructions of electron densities. It has been shown that the MEM's incorrect extrapolation of non-measured structure factors can lead to occurrence of artifacts in the resulting electron densities. The prior-derived *F* constraints can be added to the experimental data set in order to constrain the non-measured structure factors to the values calculated from the procrystal prior density.

A one-dimensional example was used to illustrate fundamental properties of the PDC. Simulated data of oxalic acid dihydrate and experimental data of sodium nitrite demonstrate the usefulness of the MEM with PDC for studies of the electron density in the chemical bond.

We believe the progress in the accuracy of the MEM reconstructions, including the presently described method, will establish the MEM as an alternative to multipole refinements. Multipole refinement is an established and powerful method for obtaining detailed information about the electron density. If a reliable multipole refinement is available, then the non-spherical density based on this multipolar model is the most informative prior that can be used in the MEM calculations. However, for certain problems, the application of the multipole refinements may become difficult or even impossible. For example, this might be the case for structures with anharmonic atomic displacements or with large correlations between structural parameters or if the number of parameters necessary to describe the structure becomes too large compared to the number of the reflections. Furthermore, at present the multipole refinement cannot be applied to modulated structures, again because of the prohibitively large number of mutually correlated modulated multipole parameters. In all these cases, the MEM can provide an attractive alternative to obtain an accurate model-free description of the electron density.

Financial support by the Deutsche Forschungsgemeinschaft is gratefully acknowledged.

References

Bader, R. F. W. (1990). *Atoms in Molecules: a Quantum Theory*. Oxford Science Publications. Oxford: Clarendon Press.
Bagautdinov, B., Luedecke, J., Schneider, M. & van Smaalen, S. (1998). *Acta Cryst.* B**54**, 626–634.
Collins, D. M. (1982). *Nature (London)*, **298**, 49–51.
Dinnebier, R. E., Schneider, M., van Smaalen, S., Olbrich, F. & Behrens, U. (1999). *Acta Cryst.* B**55**, 35–44.
Gilmore, C. J. (1996). *Acta Cryst.* A**52**, 561–589.
Gohda, T., Ichikawa, M., Gustaffson, T. & Olovsson, I. (2000). *Acta Cryst.* B**56**, 11–16.
Guillot, R., Muzet, N., Dahaoui, S., Lecomte, C. & Jelsch, C. (2001). *Acta Cryst.* B**57**, 567–578.
Iversen, B. B., Jensen, J. L. & Danielsen, J. (1997). *Acta Cryst.* A**53**, 376–387.

Jauch, W. (1994). *Acta Cryst.* A**50**, 650–652.
Jauch, W. & Palmer, A. (1993). *Acta Cryst.* A**49**, 590–591.
Jaynes, E. T. (1957). *Phys. Rev.* **106**, 620–630.
Jaynes, E. T. (1979). In *The Maximum Entropy Formalism*, edited by R. D. Levine & M. Tribus, pp. 15–118. Cambridge: MIT Press.
Jaynes, E. T. (1986). In *Maximum Entropy and Bayesian Methods in Applied Statistics*, edited by J. H. Justice, pp. 26–58. Cambridge University Press.
Palatinus, L. & van Smaalen, S. (2002). *Acta Cryst.* A**58**, 559–567.
Papoular, R. J., Collin, G., Colson, D. & Viallet, V. (2002). In *Proceedings of the 21st Workshop on Bayesian Inference and Maximum Entropy Methods in Science and Engineering*, edited by B. Fry. Melville, NY: American Institute of Physics.
Papoular, R. J., Vekhter, Y. & Coppens, P. (1996). *Acta Cryst.* A**52**, 397–407.
Roversi, P., Irwin, J. J. & Bricogne, G. (1998). *Acta Cryst.* A**54**, 971–996.
Roversi, P., Irwin, J. J. & Bricogne, G. (2002). In *Electron, Spin and Momentum Densities and Chemical Reactivity*, edited by P. G. Mezey & B. E. Roberston. Dordrecht: Kluwer Academic Publishers.
Sakata, M. & Sato, M. (1990). *Acta Cryst.* A**46**, 263–270.
Sivia, D. S. (1996). *Data Analysis – a Bayesian Tutorial.* Oxford: Clarendon Press.
Skilling, J. & Bryan, R. K. (1984). *Mon. Not. R. Astron. Soc.* **211**, 111–124.
Šlouf, M. (2001). PhD thesis, Charles University, Prague, Czech Republic.
Smaalen, S. van, Palatinus, L. & Schneider, M. (2003). *Acta Cryst.* A**59**, 459–469.
Souhassou, M., Lecomte, C., Blessing, R. H., Aubry, A., Rohmer, M.-M., Wiest, R., Marc, B. & Marraud, M. (1991). *Acta Cryst.* B**47**, 253–266.
Takata, M., Nishibori, E., Kato, K., Sakata, M. & Moritomo, Y. (1999). *J. Phys. Soc. Jpn*, **68**, 2190–2193.
Vries, R. Y. de, Briels, W. J. & Feil, D. (1994). *Acta Cryst.* A**50**, 383–391.
Vries, R. Y. de, Briels, W. J. & Feil, D. (1996). *Phys. Rev. Lett.* **77**, 1719–1722.
Wang, C.-R., Tsutomu, K., Tomiyama, T., Yoshida, T., Kobayashi, Y., Nishibori, E., Takata, M., Sakata, M. & Shinohara, H. (2001). *Angew. Chem. Int. Ed. Engl.* **40/2**, 397–399.